Langmuir

ARTICLE

pubs.acs.org/Langmuir

Self-Assembled Bilayers from the Protein HFBII Hydrophobin: Nature of the Adhesion Energy

Elka S. Basheva,[†] Peter A. Kralchevsky,[*,†] Krassimir D. Danov,[†] Simeon D. Stoyanov,[‡] Theo B. J. Blijdenstein,[‡] Eddie G. Pelan,[‡] and Alex Lips[§]

[†]Department of Chemical Engineering, Faculty of Chemistry, Sofia University, 1164 Sofia, Bulgaria

[‡]Unilever Research & Development, 3133AT Vlaardingen, The Netherlands

[§]Unilever Research & Development, Port Sunlight, Wirral, Merseyside CH63 3JW, United Kingdom

Supporting Information

ABSTRACT: The hydrophobins are a class of amphiphilic proteins which spontaneously adsorb at the air/water interface and form elastic membranes of high mechanical strength as compared to other proteins. The mechanism of hydrophobin adhesion is of interest for fungal biology and for various applications in electronics, medicine, and food industry. We established that the drainage of free foam films formed from HFBII hydrophobin solutions ends with the appearance of a 6 nm thick film, which consists of two layers of protein molecules, that is, it is a self-assembled bilayer (S-bilayer), with hydrophilic domains pointing inward and hydrophobic domains pointing outward. Its formation is accompanied by a considerable energy gain, which is much greater than that typically observed with free liquid films. The experiments at different pH show that this attraction between the "hydrophilic" parts of the HFBII molecules is dominated by the short-range hydrophobic interaction rather than by the patch-charge electrostatic attraction.

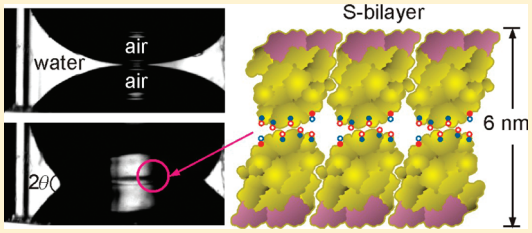

1. INTRODUCTION

The hydrophobins represent a class of relatively small proteins (about 100 amino acid residues) that are produced by filamentous fungi, including the well-known button mushrooms. In nature, these self-assembled films coat fungal structures and mediate their attachment to surfaces. Hydrophobins from the fungus *Trichoderma reesei* have been isolated, purified, and extensively studied, including the hydrophobin HFBII,[1,2] which is used in the present paper. The structure of HFBII determined from crystallized samples[3] shows that it is a single domain protein with dimensions of 2.4 × 2.7 × 3.0 nm^3. In aqueous solutions, the class II hydrophobins form dimers (at low concentrations), whereas tetramers are the dominant assemblies at mg/mL concentrations.[4−7] It was shown that the oligomerization increases with the rise of protein concentration.[5] At the surface of water, HFBII forms self-assembled monolayers.[7,8] The adsorption of this protein is not accompanied by changes in its secondary structure and ultrastructure.[7,9] Detailed reviews on the properties of hydrophobins have been published.[10−12] Their special properties have found applications as stabilizers of foams and emulsions,[13−16] as coating agents for surface modification,[17−21] and for immobilization of functional molecules at various surfaces.[17,18,22−24]

In this Article we report results from the investigation of HFBII stabilized free foam films. We established that the drainage of such a film ends with the formation of a 6 nm thick film, which consists of two layers of protein molecules; that is, it is a self-assembled bilayer (S-bilayer). The analysis of the driving force of its appearance brings information about the origin of the adhesive action of HFBII. In section 2, we describe the experimental methods. In section 3, experimental results for the effects of pH and various electrolytes are presented. Finally, in section 4, based on the obtained results, we discuss the nature of the adhesion energy. Additional details are appended as Supporting Information, including data for the effect of cations and anions on the S-bilayer formation (Appendix A), theoretical derivation of the elliptic approximation for the meniscus profile (Appendix B), and theoretical analysis of the long-range branch of disjoining pressure isotherms (Appendix C).

2. METHODS

2.1. Hydrophobin Sample Production. We used a HFBII sample produced from yeast fermentation and purified according to procedures described in detail elsewhere.[25] Briefly, *Saccharomyces cerevisiae* strain CEN.PK338 (gal1:URA3, leu2, ura3, pmt1) carried a multicopy integration vector, integrated at the rDNA locus, containing the protein coding sequence of *Trichoderma reesei* HFBII, linked to the *S. cerevisiae* SUC2 signal sequence and under control of the GAL7 promoter and leu2d selectable marker to maintain a high copy number.[26] The strain was grown in fed batch fermentations.[27] The cells were removed by centrifugation and filtration over a 0.2 μm filter, and the supernatant containing the HFBII was freeze-dried. The pH of the

Received: January 16, 2011
Revised: March 4, 2011
Published: March 17, 2011

   dx.doi.org/10.1021/la2001943 | *Langmuir* 2011, 27, 4481–4488

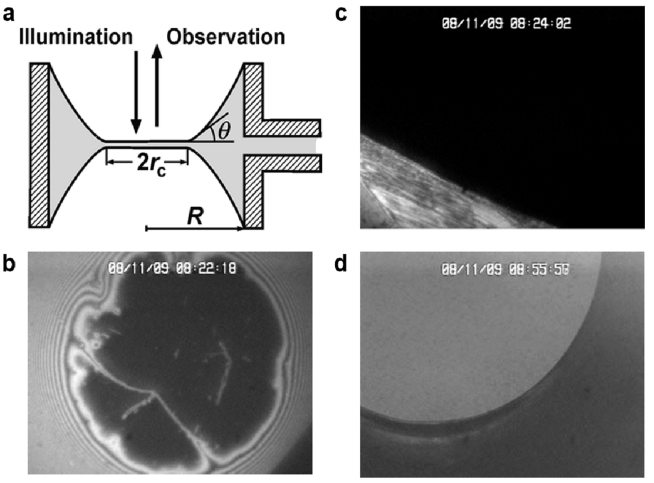

Figure 1. S-bilayer formation in SE cell. (a) Sketch of the vertical cross section of a SE cell: the foam film is formed in the central part of the cell and is observed from above in reflected light. (b) Foam film from an aqueous solution of 0.005 wt % HFBII and 25 mM $CaCl_2$; a black film of thickness $h \approx 12$ nm and average radius $r_c \approx 105$ μm is formed; it contains rodlike protein aggregates. (c) After the appearance and expansion of S-bilayer, $h \approx 6$ nm, only a part of it is seen: the black area. (d) The same S-bilayer at smaller magnification (the light gray area); the average film radius is $r_c \approx 703$ μm.

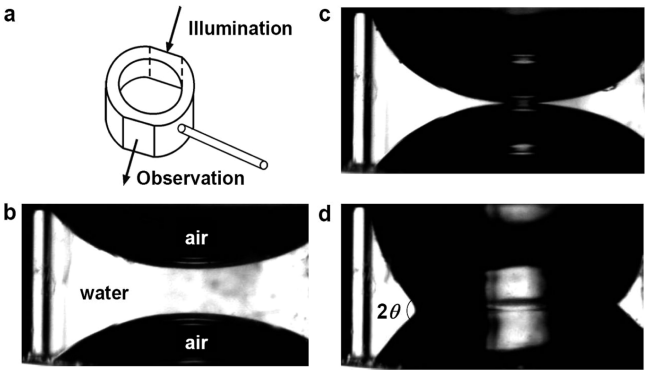

Figure 2. S-bilayer formation in Dippenaar cell. (a) Sketch of the cell: the film is formed as in SE cell, but side-view observations in transmitted light are used. (b) The two air/water surfaces are approaching each other due to the sucking of water from the biconcave drop. (c) First contact of the two surfaces. (d) The same system after the S-bilayer appearance and expansion; 2θ is the angle subtended between the two menisci at the contact line. The used protein solution is the same as that in Figure 1. See the Supporting Information for a video.

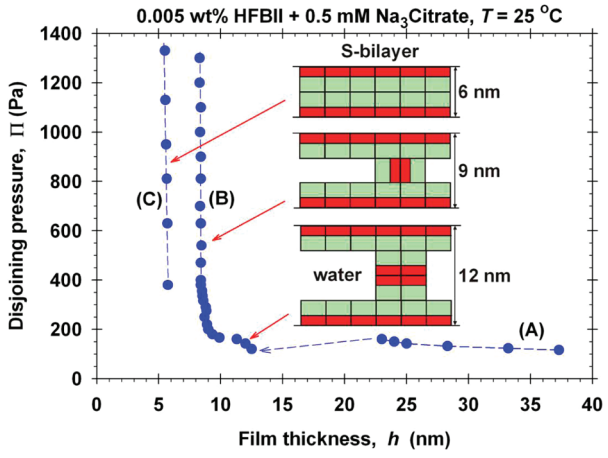

Figure 3. Plot of disjoining pressure, Π, versus film thickness, h, obtained in MJ cell. The foam film is formed from an aqueous solution of 0.005 wt % HFBII and 0.5 mM Na_3Citrate; pH = 6.0. At low pressure, the film of thickness $h \approx 12$ nm is due to vertical HFBII tetramers sandwiched between the two surface monolayers. At higher pressure, the tetramers are reoriented horizontal, which corresponds to $h \approx 9$ nm. From the top of branch B, a transition to S-bilayer of thickness $h \approx 6$ nm (branch C) occurs. The dashed lines are guides to the eye.

aqueous HFBII solutions was varied by addition of HCl or NaOH. The working temperature was 25 °C.

2.2. Scheludko–Exerowa (SE) Cell[28]. The SE cell was used in the experiments with individual free foam films (Figure 1a). First, the investigated solution is loaded in a cylindrical capillary through an orifice in its wall. Thus, a biconcave drop is formed inside the capillary. Next, liquid is sucked through the orifice and the two menisci approach each other until a liquid film is formed in the central part of the cell. By injecting or sucking liquid through the orifice, one can vary the radius of the formed film, for which the thickness can be measured by means of an interferometric method[28] of accuracy ±0.5 nm.[29] For this purpose, the light reflected from the film is supplied to a photomultiplier and computer, and the film thickness is recorded in the course of the experiment. The SE cell is placed in a closed container so that the water vapors are equilibrated with the solution and evaporation from the film is prevented. The experiments under these conditions are referred as experiments in *closed cell*. If the glass cover of the container is removed, evaporation of water from the film happens. In this case, the film can become considerably thinner. Measurements under these conditions are referred as experiments in *open cell*.

Two procedures for film formation in the SE cell have been used. First, the film is formed *immediately* after the loading of HFBII solution in the experimental cell. This procedure will be referred as the formation of films with *fresh* surfaces. The second procedure includes loading of the solution in the experimental cell and *waiting for 30 min*. After that, we form the foam film. This procedure will be termed formation of films with *aged* surfaces.

2.3. Dippenaar Cell[30]. The Dippenaar cell is very similar to the SE cell by construction and operational principle, but side-view observations are used (Figure 2a). For this reason, two opposite parts of the cylindrical wall are polished flat to avoid optical distortion of the image by the cylindrical wall. In our contact angle measurements, we simultaneously used side- and top-view observations of the same film in a Dippenaar cell to compare the two different approaches for determining the contact angle at the film periphery (see Appendix B in the Supporting Information). The construction of the SE and Dippenaar cells does not allow one to apply capillary pressures higher than ca. 85 Pa in closed cell. In open cell, the acting hydrodynamic pressure can be higher, with its magnitude being proportional to the evaporation rate.[31]

2.4. Mysels–Jones (MJ) Cell[32]. The MJ cell allows one to press the two film surfaces against each other at higher pressures, up to 1500 Pa in our experiments. The cylindrical film holder is made of porous glass, so that the solution is supplied in the cell through the pores. In our experiments, the average pore diameter was relatively large, 40 μm, to avoid blocking of pores by protein aggregates. The MJ cell enables one to measure disjoining-pressure versus film-thickness isotherms, $\Pi(h)$; see Figures 3 and 4. Experimentally, the applied pressure (which equals Π at equilibrium) is varied and the respective equilibrium value of h is determined form the intensity of the light reflected from the film, using the same interference method as with the SE cell. A detailed description of the used MJ cell and of its operational procedure can be found elsewhere.[33]

dx.doi.org/10.1021/la2001943 |*Langmuir* 2011, 27, 4481–4488

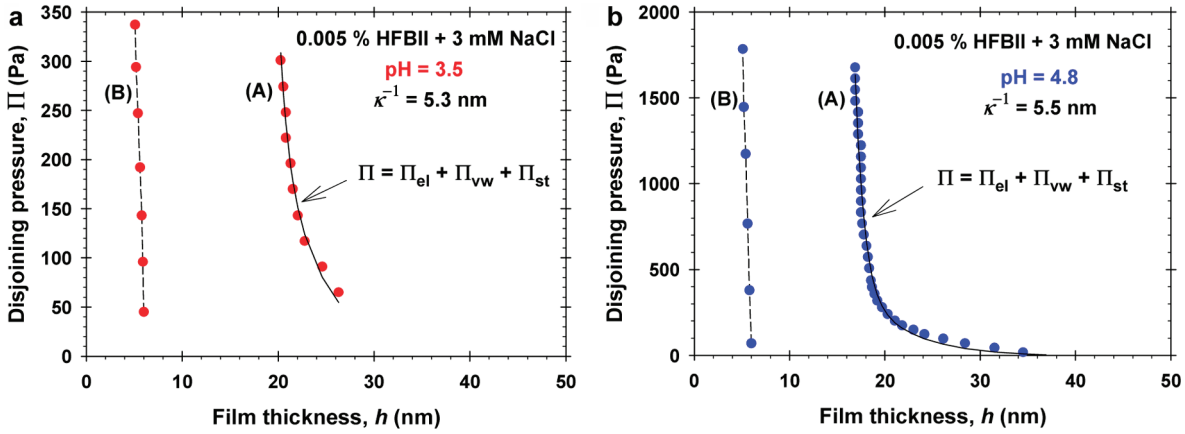

Figure 4. Effect of pH on the S-bilayer formation. Experimental data for Π versus h, as in Figure 3, obtained at different pH values in the presence of 3 mM NaCl. (a) pH = 3.5; (b) pH = 4.8. The solid line is the best fit of the branch A with eqs 3 and 4; κ is the Debye screening parameter. Branch B, corresponding to $h \approx 6$ nm, represents S-bilayer.

3. EXPERIMENTAL RESULTS AND DISCUSSION

3.1. Experiments in SE Cell. Here, we investigate the formation of S-bilayers as a result of thinning of foam films from aqueous solutions of 5×10^{-3} wt % HFBII + 25 mM $CaCl_2$. (S-bilayers appear also in the presence of other electrolytes; see Appendix A in the Supporting Information.) After a foam film is formed in the SE cell (Figure 1a), its thickness gradually decreases due to the drainage of liquid from the film toward the surrounding meniscus. In closed cell, the film drainage stops when the thickness becomes ≈15 nm. The obtained film contains rodlike HFBII aggregates. Further thinning can be observed if we open the experimental cell, which leads to evaporation of water from the film. Then, the film thins down to 12 nm (Figure 1b).

A few minutes after the formation of the 12 nm film, a sudden and fast transition to thickness ≈ 6 nm occurs. Because the dimension of the HFBII molecule along the normal to the interface is ≈3 nm, the film of thickness 6 nm consists of two layers of protein molecules; that is, it is a self-assembled bilayer (S-bilayer). The latter is a compact membrane of HFBII, which (to some extent) resembles the S-layer, a self-assembled protein monolayer[34] found on the cell surface of some common bacteria and archaea.

During the S-bilayer formation, the film radius spontaneously increases from about 100 μm to ≈700 μm (and even larger in other experiments; see Appendix A in the Supporting Information). This considerable increase of the film area (about 50 times) gives evidence that the formation of S-bilayer is accompanied by a significant energy gain; that is, the adhesion of the two HFBII monolayers is energetically very favorable. In Figure 1c, only a small part of the formed S-bilayer is seen. It looks black because the reflection from a 6 nm thick film is rather low. To measure the radius of the latter film, we used lower magnification (Figure 1d) where the S-bilayer looks gray because of the different aperture and illumination.

The formed S-bilayers were stable; they did not break during the whole period of our observations of a given film, up to 12 h. Only in some of the experiments with $AlCl_3$ and *fresh* film surfaces, the formed bilayers ruptured in the process of their formation (see Appendix A in the Supporting Information), which can be attributed to an incomplete consolidation of the elastic HFBII membranes on the film surfaces. (The respective films with *aged* film surfaces were stable.)

3.2. Experiments in Dippenaar Cell. Video frames from the process of approaching of the two film surfaces and the S-bilayer formation after their contact are shown in Figure 2. (See the Supporting Information for the whole movie.) By sucking of water from the Dippenaar cell[30] through the side capillary (Figure 2a), we bring the two film surfaces closer (Figure 2b) until they touch each other (Figure 2c). Soon after that, we observe the formation of an S-bilayer, which is manifested as a fast and considerable expansion of the contact zone. The state with the S-bilayer is stable; configurations such as that in Figure 2d did not change during the whole period of subsequent observations (from 1 to 12 h).

From the side-view photographs, like that in Figure 2d, we measured the contact angle θ by using a goniometer. Mean arithmetic was taken for the values of θ determined from the left- and right-hand side meniscus profiles. For the system in Figure 2, the goniometric method yields $\theta = 50.0° \pm 1.4°$, which is an average from five experiments.

We developed also another method for determination of θ from the radius r_c of the three-phase contact line around the film. This method (applicable with both SE and Dippenaar cells) is described in Appendix B in the Supporting Information. There, an elliptic approximation for the meniscus profile is used to derive the following expression for θ:

$$\tan\theta = \frac{r_c/R}{(1 - r_c^2/R^2)^2} \qquad (1)$$

R is the radius of the inner cylindrical wall of the experimental cell; see Figure 1a for the notations. In our case, R = 1.2 mm. Substituting the experimental values of R and r_c in eq 1, we calculated $\theta = 51.5° \pm 1.1°$, which is average for the same five experiments, for which the goniometric method was applied (see above). The values of θ obtained using the two different methods are in good agreement.

3.3. Contact Angle and Interaction Energy. The energy of attraction per unit area of the film, ΔW, is related to the film contact angle, θ, by means of the equation:[35]

$$\Delta W = 2\sigma(1 - \cos\theta) \qquad (2)$$

where σ is the tension of the HFBII membrane at the meniscus surface. Because the S-bilayer expands during its formation, the

dx.doi.org/10.1021/la2001943 |*Langmuir* 2011, 27, 4481–4488

menisci around it are compressed and sometimes wrinkles are observed. Experiments with HFBII monolayers in a Langmuir trough[16] indicate that the tension of a dense monolayer (membrane), just before its wrinkling, is $\sigma \approx 12$ mN/m. Substituting the latter value and $\theta \approx 51°$ in eq 2, we obtain $\Delta W = 8.9$ mJ/m^2. This is only an estimate, because the tension of an elastic membrane can vary depending on its degree of extension, unlike the equilibrium surface tension of a surfactant solution.

The equilibrium contact angle of the S-bilayer, $\theta \approx 51°$, is much greater than the contact angles of foam films stabilized by conventional surfactants, which are typically in the range $1-3°$ for nonionic surfactants[36,37] and could reach a maximum of 10° for ionic surfactants at high salt concentrations.[35,38] The interaction energy $\Delta W = 8.9$ mJ/m^2 estimated above is also by order of magnitude greater than the greatest values of ΔW measured with Newton black soap films.[35] This significant difference indicates that in the case of the S-bilayer we are encountering an effect of different physical nature (see below).

Multiplying ΔW with the area per molecule, $A_p = 2.4 \times 2.7 = 6.48$ nm^2, we obtain $\Delta W_2 = 5.8 \times 10^{-20}$ J $\approx 14kT$ per pair of interacting HFBII molecules (k, Boltzmann constant; T, temperature). $\Delta W_2 \equiv A_p \Delta W$ is the energy of adhesion of the *hydrophilic* parts of two protein molecules belonging to the two opposite surfaces of an S-bilayer.

Here, for the first time, the formation of a protein bilayer with such a high energy gain is observed as evidenced by the spontaneous increase of the film area ($\geq$50 times) and the large *equilibrium* contact angle of the formed film ($\theta > 50°$). The formation of black films, which represent protein bilayers, has been observed many times, but never with such large contact angles. For example, the maximum equilibrium contact angles of protein black films reported in the literature are $\theta = 0.9°$ in the case of bovine serum albumin (BSA) + 0.15 M NaCl,[39] $\theta = 1.7°$ for α-chymotrypsin + 0.1 mM NaCl,[40] and 2.7° for α-lactalbumin.[41]

Because the surfaces of the protein black films adhere to each other, there is contact angle hysteresis, so that the *advancing* angle (at a shrinking contact line and detaching film surfaces), θ_{adv}, can be considerably greater than the equilibrium one. The following maximum values of the advancing angles have been reported for different systems: $\theta_{adv} = 1.4°$ for BSA,[39] $\theta_{adv} = 1.8°$ for human serum albumin,[40] and $\theta_{adv} \approx 7°$ for α-lactalbumin.[41] The greatest value of the advancing angle was detected for β-casein black films in the presence of bridging Ca^{2+} ions: $\theta_{adv} \approx 90°$ at a rate of contact line shrinking ≤ 10 μm/s.[42]

In the case of HFBII, the spontaneous increase of the area of a forming S-bilayer eventually stops at a certain value of the film radius, r_c, and contact angle, θ. After that, the values of r_c and θ remain constant during the whole period of observations (up to 12 h) and are considered as equilibrium ones. Next, if we begin to pump solution in the Plateau border around the film, the contact angle increases at *immobile* contact line (at fixed r_c). When the contact angle approaches 90°, the two film surfaces suddenly detach. Under such circumstances, there is no definite value of the advancing contact angle, θ_{adv}. After their detachment, the two film surfaces have an irregular shape, which gradually relaxes to a spherical meniscus.

The adhesive interactions between the HFBII molecules lead to their irreversible aggregation in the bulk of solution. As mentioned above, initially the tetramers are the most abundant oligomers in the mg/mL concentration range.[4−7] The mean aggregate size increases with time, which was studied by light scattering.[13] Micrometer-sized and larger aggregates are directly visible by optical microscopy.[43] They can be destroyed by sonication of the solution, but after that the aggregate growth commences again.

The attraction between the "hydrophilic" parts of the HFBII molecules (that is responsible for the S-bilayer formation) favors not only the protein aggregation in the bulk of solution but also the attachment of the formed aggregates to the interfacial protein adsorption layer. Micrometer-sized rodlike (fibrillar) aggregates were observed at the surfaces of aqueous hydrophobin solutions,[4] especially in the cases with added electrolytes.[43]

3.4. Experiments in MJ Cell. Figure 3 shows a typical experimental $\Pi(h)$ dependence (Π is disjoining pressure = surface force per unit area;[44,45] h is the film thickness) obtained by the MJ cell.[32] The foam film is formed from a solution of 0.005 wt % HFBII and 0.5 mM Na_3Citrate. The experimental curve consists of three branches which are denoted A, B, and C. Branch A corresponds to large h and relatively small Π; its physical interpretation is similar to that of the A branches in Figure 4 (see below). The transition from branch A to branch B occurs by the appearance and expansion of dark spots (of smaller thickness) in the foam film. Branch B begins at $h \approx 12$ nm, which corresponds to the thickness of two HFBII adsorption monolayers ($2 \times 3 = 6$ nm) plus the size of sandwiched HFBII tetramers (6 nm); see the lower inset in Figure 3. (Films of thickness 12 nm are often observed in the SE cell; see Figure 1b and Appendix A in the Supporting Information.) Upon a further increase of pressure, h decreases from 12 to 9 nm. Such a transition can be explained with a forced reorientation of the sandwiched tetramers, which are anisodiametric particles of dimensions $6 \times 6 \times 3$ nm. Indeed, if the short (3 nm) side of the HFBII tetramer is oriented along the film thickness, we obtain $h = 3 + 2 \times 3 = 9$ nm (the middle inset in Figure 3). Finally, at pressure $\Pi \approx 1300$ Pa, the film undergoes a transition to S-bilayer ($h \approx 6$ nm) which, as always, appears with a sudden and fast expansion of the film area; see branch C and the upper inset in Figure 3.

3.5. Effect of pH on the S-Bilayer Formation. $\Pi(h)$ isotherms were obtained by the MJ cell with films from solutions containing 0.005 wt % HFBII plus 3 mM added NaCl or 1 mM added Na_2SO_4 at various pH values. For both electrolytes, in all experiments, we observed the formation of S-bilayer of thickness ≈ 6 nm at the end of film thinning irrespective of the pH value, which was 3.5, 4.8, 5.8, 6.5, 7.5, and 8.2 in these experiments. In most of them, the S-bilayer was the only observed stable state of the film. In some experiments at pH < 5.5, the formation S-bilayer (the branch B in Figure 4a and b) was preceded by the appearance of thicker stable films; see branch A in Figure 4a and b. The appearance of the A branch is more typical for solutions containing NaCl; its height considerably varies in different experiments at the same solution composition.

A possible hypothesis for explanation of the long-range A branches in Figures 3 and 4 is that they are due to a steric (osmotic overlap) repulsion induced by HFBII aggregates adherent to the HFBII monolayers at the film surfaces. As mentioned above, HFBII exhibits a tendency to form rodlike aggregates of nanometer, and even of micrometer, size (see e.g. Figure 2b). Their average length depends on the HFBII concentration and on the solution's age (after the initial sonication).[5,12] Even at low surface concentrations, the adsorbed aggregates can produce a significant steric repulsion.[46]

Table 1. Critical Concentration for S-Bilayer Formation, C_{SBL}

anions[a]		cations[a]	
electrolyte	C_{SBL}, mM	electrolyte	C_{SBL}, mM
NaI	100		
TMABr[b]	100	**TMA**Br	100
NaCl	100	**Na**Cl	100
Na_2**SO**$_4$	1	**Ca**Cl_2	25
Na_3**Citrate**[c]	0.5	**Al**Cl_3	10

[a] The respective anions and cations are typed bold. [b] TMABr = Tetramethylammonium bromide. [c] The concentration of $Citrate^{3-}$ is 0.135 mM (pH = 6).

To check the above hypothesis, we fitted the A branches of the experimental $\Pi(h)$ dependences in Figure 4a and b with the expression:

$$\Pi = \Pi_{el} + \Pi_{vw} + \Pi_{st} \quad (3)$$

For the electrostatic, Π_{el}, and van der Waals, Π_{vw}, components of disjoining pressure, we used known theoretical expressions;[45] see Appendix C in the Supporting Information. The data comply with a steric component of disjoining pressure, Π_{st}, that exponentially decays with the film thickness h:

$$\Pi_{st} = A \exp\left[-b(h - h_a)\right] \quad (4)$$

Here, h_a = 6 nm is the net thickness of the HFBII adsorption layers at the two film surfaces; the parameters A and b have been determined from the fits as adjustable parameters. For the two pH values in Figure 4, we obtained the same b = 1.1 nm^{-1}, whereas the values of A are different: 1.0×10^9 Pa in Figure 4a versus 1.3×10^8 Pa in Figure 4b. The latter could be explained with irreproducible surface density of the attached aggregates in different runs because of the rather low protein concentration (0.005 wt %). All three terms in eq 3 give comparable contributions to Π; for details, see Appendix C in the Supporting Information.

3.6. Effect of the Type of Electrolyte. We investigated whether and how the type and concentration of electrolyte affect the formation of S-bilayers. All experiments were carried out in the SE cell at 5×10^{-3} wt % HFBII concentration at the solutions' natural pH (5.5−6.0). A detailed description of the experimental results is given in Appendix A in the Supporting Information. In Table 1, the experimental critical concentration for S-bilayer appearance in the SE cell, C_{SBL}, is listed for various electrolytes. The increase of the valence of both anions and cations leads to a decrease in C_{SBL}. In this respect, anions, such as SO_4^{2-} and $Citrate^{3-}$, produce a stronger effect than cations as Ca^{2+} and Al^{3+}. This can be explained with the fact that at pH = 5.5−6.0 the net charge of the HFBII monolayer is positive (the isoelectric point is at pH = 6.7; see below); that is, the anions play the role of counterions. The easiest formation of S-bilayer was observed in the presence of $Citrate^{3-}$ ions with respect to (i) low electrolyte concentration; (ii) in closed cell, without water evaporation from the film, (iii) at relatively small film radius (≈100 μm), and (iv) soon after the film formation.

In general, the electrolytes produce a twofold effect. First, they suppress the electrostatic repulsion between the two film surfaces, promoting their close contact and the formation of S-bilayer. Second, the electrolytes favor the formation of HFBII aggregates, which adsorb at the film surfaces and impede the formation of S-bilayer. In other words, the addition of electrolyte lowers the electrostatic barrier, Π_{el}, but increases the steric barrier, Π_{st}. Consequently, to promote the formation of S-bilayer, the electrolyte concentration should be high enough to suppress the electrostatic repulsion but it should not be too high to avoid the blockage of film thinning by adsorbed aggregates.

The values of C_{SBL} in Table 1 have been obtained by experiments in the SE cell at a relatively small applied pressure difference (<85 Pa). The MJ cell allows one to apply greater pressure differences, which leads to the appearance of S-bilayers at lower electrolyte concentrations due to overcoming of the electrostatic and steric barriers to film thinning.

4. DISCUSSION ON THE NATURE OF THE ADHESIVE ENERGY

The experimental data presented above imply that an intensive attraction exists between the *hydrophilic* parts of the HFBII molecules, which leads to the spontaneous formation of a S-bilayer (see the upper inset in Figure 3) as a final stage of film thinning. Another consequence of this attraction is the experimentally observed growth of aggregates in the aqueous HFBII solutions and the adhesion of these aggregates to the interfacial protein monolayers. There are (at least) two possible explanations of the attraction between the hydrophilic parts of the HFBII molecules.

First, the effect could be explained with the electrostatic *patch-charge attraction*, which is due to the presence of an equal number of positive and negative charged groups arranged in a mosaic pattern at each of the two film surfaces in such a way that unlike charges face each other. This effect was theoretically described[47] and proposed as an explanation of the attractive energy in the Newton black soap films.[48] Recently, this interaction was investigated by the colloidal-probe AFM technique.[49] The structure of the HFBII molecule indicates that both negative and positive charges are present at that part of the HFBII molecule, which is facing water in the adsorption layer (Figure 5). In principle, this makes possible the existence of patch-charge attraction between the two adsorption layers.

A second source of attraction can be the short-range *hydrophobic interaction* due to the presence of amino-acid residues with hydrophobic side chains on the water-facing part of the HFBII molecule. There are six such residues: Ala37, Ile38, Phe39, Ala41, Ala44, and Leu 51 (Figure 5). Hence, the hydrophobic attraction[45,50,51] can also be operative. It is expected to be present at every pH, providing the thinning film has overcome the barrier due to the electrostatic and steric repulsion.

In contrast, the patch-charge attraction is expected to appear in the vicinity of the isoelectric point, where there are equal numbers of positive and negative groups on each of the two film surfaces. Calculations by the program ProtParam, based on the protein primary structure data, predicted that the isoelectric point is at pH = 6.7 for an *isolated* protein molecule in water.[6,52] The electrophoretic measurements with HFBII-covered *bubbles* give a slightly higher isoelectric point, pI = 7.5, which can be explained with the fact that a part of the anionic groups (Asp20, Asp25, and Asp59; Figure 5) are embedded in the closely packed protein adsorption layer that covers the bubble surface.[43]

The results for the Π versus h dependencies reported above (see, e.g., Figure 4) show that S-bilayers are formed irrespective of the pH value in the investigated interval, 3.5 ≤ pH ≤ 8.5. The latter fact indicates that the physical origin of the adhesive force

dx.doi.org/10.1021/la2001943 |*Langmuir* 2011, 27, 4481–4488

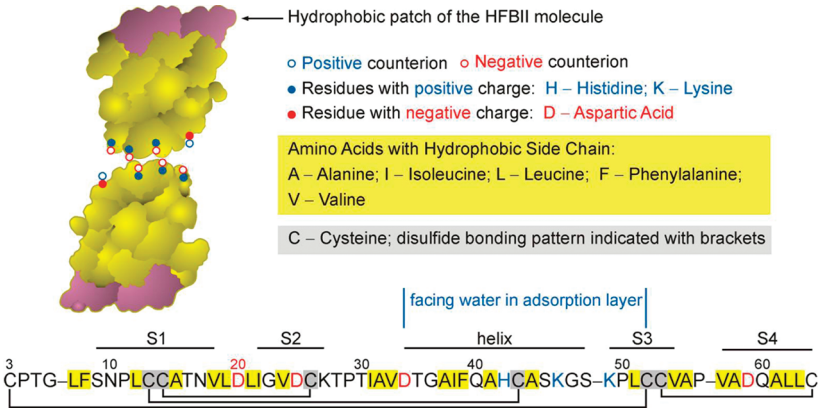

Figure 5. Interaction of two HFBII molecules in an S-bilayer in relation to the protein structure. Sketch of two interacting HFBII molecules: the ionizable groups in the zone of contact are shown together with bound counterions. The HFBII amino acid sequence between the first and last Cys residues is also shown with residue numbering and secondary structures.[2,10,11] The portion of the sequence that is facing the water phase in a dense HFBII adsorption layer at the air/water interface is denoted. Upon contact, the ionizable groups are neutralized by condensed counterions, whereas the hydrophobic groups are able to engender an adhesive force that is the most probable reason for the S-bilayer formation at various pH values.

in the S-bilayer is the hydrophobic attraction, rather than the patch-charge attraction. Hence, the S-bilayers are different from the Newton black films[35,48] by the source of their attractive energy. This could be related also to the fact the contact angles of S-bilayers ($\theta \approx 50°$, see above) are considerably greater than those of Newton black films ($\theta \leq 10°$).[35]

The formation of an S-bilayer was observed in the presence of various ions, both monovalent and multivalent, and at various ionic strengths: from 0.5 mM Na_3Citrate (Table 1) to 500 mM TMAB (Appendix A, Supporting Information). All these results indicate that in the considered case the main role of the electrolyte is to eliminate the electrostatic repulsion between the two film surfaces by suppressing the diffuse electric double layers and by surface-charge neutralization due to counterion binding. This allows the surfaces to come sufficiently close to each other to enable the short-range hydrophobic attraction to initiate the S-bilayer formation.

The energy of short-range hydrophobic attraction per unit area of a plane-parallel film can be estimated from the formula:[45]

$$W_{hb} = -2w\, e^{-H/\lambda_0} \quad (5)$$

$H = h - h_a$ is the distance between the two hydrophobic surfaces; typically, the coefficient is $w = 10-50$ mJ/m^2, and $\lambda_0 = 1-2$ nm. Setting $H = 0$ in eq 5, we can estimate the magnitude of the hydrophobic adhesion energy of two protein molecules, like those sketched in Figure 5:

$$|\Delta W_2| = 2w\alpha A_p \quad (6)$$

Here, $A_p = 6.48$ nm^2 is the area per HFBII molecule and α is the fraction of this area where hydrophobic groups belonging to the two interacting molecules are in contact. Substituting $|\Delta W_2| = 5.8 \times 10^{-20}$ J (see above) in eq 6 along with the mean value $w = 30$ mJ/m^2, we obtain $\alpha = 0.15$, which is a reasonable value having in mind that not all amino acid residues in the contact zone have hydrophobic side chains (Figure 5).

An upper estimate for the hydrophobic adhesion energy can be obtained from the maximum measured energy:[50,51] $2w \approx 100$ mJ/m^2, multiplied by the maximal contact area of two HFBII molecules, 6.48 nm^2, which gives 6.48×10^{-19} J, that, is $157kT$. As mentioned above, the hydrophobic adhesion energy per pair of HFBII molecules is expected to be lower, because only a part of the amino acid residues expressed at the protein/water boundary have hydrophobic side chains; see the estimate based on eq 6.

The adsorption of various proteins on surface films of hydrophobin was recently investigated, and it was concluded that the surface adhesion is due to selective Coulombic charge interactions.[21] The data reported there are not in contradiction with our conclusions about the role of the short-range hydrophobic attraction. Except at the isoelectric point, an electrostatic barrier exists (see Appendix C in the Supporting Information), which impedes the protein adsorption, as well as the formation of S-bilayers in the SE cell, as reported above. In our experiments with the MJ cell, we applied an additional external pressure to overcome the electrostatic (and steric) barriers. In the experiments on protein adsorption, such external force is missing, so that the adsorbing molecules can overcome the barrier only in the vicinity of the isoelectric point, as indicated by the peaks in the adsorption versus pH dependencies in ref 21.

In summary, the obtained results support the conclusion that the energy of adhesion of the two monolayers in an S-bilayer is dominated by the hydrophobic attraction. The electrostatic interaction is repulsive and impedes the S-bilayer formation, but its effect can be suppressed owing to the binding of counterions. In this respect, efficient are electrolytes containing Cl^-, SO_4^{2-}, and Citrate^{3-} ions, which neutralize the predominantly positive ionizable groups (of Lys and His), present on the water-facing side of the HFBII adsorption layer. The obtained new information (the S-bilayer attraction and the repulsion due to adherent protein oligomers) is important for the control of longevity of hydrophobin-stabilized foams and emulsions. The hydrophobic origin of the adhesive force is essential for the application of hydrophobins as immobilizing agents: The immobilized functional molecule or particle should be hydrophobic, and appropriate electrolytes have to be used to suppress the electrostatic repulsion.

■ ASSOCIATED CONTENT

Supporting Information. Appendix A, effect of cations and anions on the S-bilayer formation; Appendix B, Elliptic approximation for the meniscus profile; Appendix C, long-range

dx.doi.org/10.1021/la2001943 |*Langmuir* 2011, 27, 4481–4488

branch of disjoining pressure; and a Movie showing the whole process of S-bilayer formation in a Dippenaar cell (see Figure 2). This material is available free of charge via the Internet at http://pubs.acs.org.

AUTHOR INFORMATION

Corresponding Author
*Telephone: (+359) 2-8161262. Fax: (+359) 2-9625643. E-mail: pk@lcpe.uni-sofia.bg.

ACKNOWLEDGMENT

The authors gratefully acknowledge the support from Unilever Research, from the Project DID 02-18/2009 with the Bulgarian National Science Fund, and from COST Action D43 of ESF. The authors are grateful to Ms. Mariana Paraskova for her assistance in figure preparation.

REFERENCES

(1) Nakari-Setälä, T.; Aro, N.; Ilmén, M.; Muñoz, G.; Kalkkinen, N.; Penttilä, M. Differential expression of the vegetative and spore-bound hydrophobins of Trichoderma reesei — cloning and characterization of the HFBII gene. *Eur. J. Biochem.* **1997**, *248*, 415–423.

(2) Hakanpää, J.; Szilvay, G. R.; Kaljunen, H.; Maksimainen, M.; Linder, M.; Rouvinen, J. Two crystal structures of Trichoderma reesei hydrophobin HFBI—The structure of a protein amphiphile with and without detergent interaction. *Protein Sci.* **2006**, *15*, 2129–2140.

(3) Hakanpää, J.; Paananen, A.; Askolin, A.; Nakari-Setälä, T.; Parkkinen, T.; Penttilä, M.; Linder, M. B.; Rouvinen, J. Atomic resolution structure of the HFBII hydrophobin, a self-assembling amphiphile. *J. Biol. Chem.* **2004**, *279*, 534–539.

(4) Torkkeli, M.; Serimaa, R.; Ikkala, O.; Linder, M. Aggregation and self-assembly of hydrophobins from Trichoderma reesei: low-resolution structural models. *Biophys. J.* **2002**, *83*, 2240–2247.

(5) Szilvay, G. R.; Nakari-Setälä, T.; Linder, M. B. Behavior of Trichoderma reesei hydrophobins in solution:interactions, dynamics, and multimer formation. *Biochemistry* **2006**, *45*, 8590–8598.

(6) Kisko, K.; Szilvay, G. R.; Vainio, U.; Linder, M. B.; Serimaa, R. Interactions of Hydrophobin Proteins in Solution Studied by Small-Angle X-Ray Scattering. *Biophys. J.* **2008**, *94*, 198–206.

(7) Kisko, K.; Szilvay, G. R.; Vuorimaa, E.; Lemmetyinen, H.; Linder, M. B.; Torkkeli, M.; Serimaa, R. Self-assembled films of hydrophobin proteins HFBI and HFBII studied in situ at the air/water interface. *Langmuir* **2009**, *25*, 1612–1619.

(8) Szilvay, G. R.; Paananen, A.; Laurikainen, K.; Vuorimaa, E.; Lemmetyinen, H.; Peltonen, J.; Linder, M. B. Self-assembled hydrophobin protein films at the air-water interface: structural analysis and molecular engineering. *Biochemistry* **2007**, *46*, 2345–2354.

(9) Askolin, S.; Linder, M.; Scholtmeijer, K.; Tenkanen, M.; Penttila, M.; de Vocht, M. L.; Wösten, H. A. B. Interaction and comparison of a class I hydrophobin from Schizophyllum commune and class II hydrophobins from Trichoderma reesei. *Biomacromolecules* **2006**, *7* 1295–1301.

(10) Linder, M. B.; Szilvay, G. R.; Nakari-Setälä, T.; Penttila, M. Hydrophobins: the protein-amphiphiles of filamentous fungi. *FEMS Microbiol. Rev.* **2005**, *29*, 877–896.

(11) Sunde, M.; Kwan, A. H. Y.; Templeton, M. D.; Beever, R. E.; Mackay, J. P. Structural analysis of hydrophobins. *Micron* **2008**, *39*, 773–784.

(12) Linder, M. B. Hydrophobins: proteins that self assemble at interfaces. *Curr. Opin. Colloid Interface Sci.* **2009**, *14*, 356–363.

(13) Cox, A. R.; Cagnol, F.; Russell, A. B.; Izzard, M. J. Surface properties of class II hydrophobins from Trichoderma reesei and influence on bubble stability. *Langmuir* **2007**, *23*, 7995–8002.

(14) Cox, A. R.; Aldred, D. L.; Russell, A. B. Exceptional stability of food foams using class II hydrophobin HFBII. *Food Hydrocolloids* **2009**, *23*, 366–376.

(15) Tchuenbou-Magaia, F. L.; Norton, I. T.; Cox, P. W. Hydrophobins stabilised air-filled emulsions for the food industry. *Food Hydrocolloids* **2009**, *23*, 1877–1885.

(16) Blijdenstein, T. B. J.; de Groot, P. W. N.; Stoyanov, S. D. On the link between foam coarsening and surface rheology: why hydrophobins are so different. *Soft Matter* **2010**, *6*, 1799–1808.

(17) Qin, M.; Wang, L.-K.; Feng, X.-Z.; Yang, Y.-L.; Wang, R.; Wang, C.; Yu, L.; Shao, B.; Qiao, M.-Q. Bioactive surface modification of mica and poly(dimethylsiloxane) with hydrophobins for protein immobilization. *Langmuir* **2007**, *23*, 4465–4471.

(18) Asakawa, K.; Tahara, S.; Nakamichi, M.; Takehara, K.; Ikeno, S.; Linder, M.; Haruyama, T. The amphiphilic protein HFBII as a genetically taggable molecular carrier for the formation of a self-organized functional protein layer on a solid surface. *Langmuir* **2009**, *25*, 8841–8844.

(19) Lumsdon, S. O.; Green, J.; Stieglitz, B. Adsorption of hydrophobin proteins at hydrophobic and hydrophilic interfaces. *Colloids Surf., B* **2005**, *44*, 172–178.

(20) Li, X.; Hou, S.; Feng, X.; Yu, Y.; Ma, J.; Li, L. Patterning of neural stem cells on poly(lactic-co-glycolic acid) film modified by hydrophobin. *Colloids Surf., B* **2009**, *74*, 370–374.

(21) Wang, Z.; Lienemann, M., M.; Linder, M. B. Mechanisms of protein adhesion on surface films of hydrophobin. *Langmuir* **2010**, *26*, 8491–8496.

(22) Linder, M. B.; Qiao, M.; Laumen, F.; Selber, K.; Hyytiä, T.; Nakari-Setälä, T.; Penttilä, M. E. Efficient purification of recombinant proteins using hydrophobins as tags in surfactant-based two-phase systems. *Biochemistry* **2004**, *43*, 11873–11882.

(23) Zhao, Z.-X.; Qiao, M.-Q.; Yin, F.; Shao, B.; Wu, B.-Y.; Wang, Y.-Y.; Wang, X.-S.; Qin, X.; Li, S.; Yu, L.; Chen, Q. Amperometric glucose biosensor based on self-assembly hydrophobin with high efficiency of enzyme utilization. *Biosens. Bioelectron.* **2007**, *22*, 3021–3027.

(24) Linder, M.; Szilvay, G. R.; Nakari-Setälä, T.; Söderlund, H.; Penttilä, M. Surface adhesion of fusion proteins containing the hydrophobins HFBI and HFBII from Trichoderma reesei. *Protein Sci.* **2002**, *11*, 2257–2266.

(25) Bailey, M.; Askolin, S.; Hörhammer, N.; Tenkanen, M.; Linder, M.; Penttilä, M.; Nakari-Setälä, T. Process technological effects of deletion and amplification of hydrophobins I and II in transformants of Trichoderma reesei. *Appl. Microbiol. Biotechnol.* **2002**, *58*, 721–727.

(26) Lopes, T. S.; de Wijs, I. J.; Steenhauer, S. I.; Verbakel, J.; Planta, R. J. Factors affecting themitotic stability of high-copy-number integration into the ribosomal DNA of Saccharomyces cerevisiae. *Yeast* **1996**, *12*, 467–477.

(27) Thomassen, Y. E.; Meijer, W.; Sierkstra, L.; Verrips, C. T. Large-scale production of VHH antibody fragments by Saccharomyces cerevisiae. *Enzyme Microb. Technol.* **2002**, *30*, 273–278.

(28) Sheludko, A. Thin liquid films. *Adv. Colloid Interface Sci.* **1967**, *1*, 391–464.

(29) Bergeron, V.; Radke, C. J. Equilibrium measurements of oscillatory disjoining pressures in aqueous foam films. *Langmuir* **1992**, *8*, 3020–3026.

(30) Dippenaar, A. The destabilization of froth by solids: I. The mechanism of film rupture. *Int. J. Miner. Process.* **1982**, *9*, 1–14.

(31) Kralchevsky, P. A.; Nagayama, K. *Particles at Fluid Interfaces and Membranes*; Elsevier: Amsterdam, 2001; Chapter 14.

(32) Mysels, K. J.; Jones, M. N. Direct measurement of the variation of double-layer repulsion with distance. *Discuss. Faraday Soc.* **1966**, *42*, 42–50.

(33) Dimitrova, T. D.; Leal-Calderon, F.; Gurkov, T. D.; Campbell, B. Disjoining pressure vs thickness isotherms of thin emulsion films stabilized by proteins. *Langmuir* **2001**, *17*, 8069–8077.

(34) Messner, P.; Sleytr, U. Crystalline bacterial cell-surface layers. *Adv. Microb. Physiol.* **1992**, *33*, 213–275.

(35) De Feijter, J. A.; Vrij, A. Contact angles in thin liquid films. II. Contact angle measurements in Newton black soap films. *J. Colloid Interface Sci.* **1978**, *64*, 269–277.
(36) Lobo, L. A.; Nikolov, A. D.; Dimitrov, A. S.; Kralchevsky, P. A.; Wasan, D. T. Contact angle of air bubbles attached to an air-water surface in foam applications. *Langmuir* **1990**, *6*, 995–1001.
(37) Basheva, E. S.; Kralchevsky, P. A.; Danov, K. D.; Ananthapadmanabhan, K. P.; Lips, A. The colloid structural forces as a tool for particle characterization and control of dispersion stability. *Phys. Chem. Chem. Phys.* **2007**, *9*, 5183–5198.
(38) Kralchevsky, P. A.; Nikolov, A. D.; Ivanov, I. B. Film and line tension effects on the attachment of particles to an interface: IV. Experimental studies with bubbles in solutions of dodecyl sodium sulfate. *J. Colloid Interface Sci.* **1986**, *112*, 132–143.
(39) Marinova, K. G.; Gurkov, T. D.; Velev, O. D.; Ivanov, I. B.; Campbell, B.; Borwankar, R. P. The role of additives for the behaviour of thin emulsion films stabilized by proteins. *Colloids Surf., A* **1997**, *123*, 155–167.
(40) Yampolskaya, G.; Platikanov, D. Proteins at fluid interfaces: adsorption layers and thin liquid films. *Adv. Colloid Interface Sci.* **2006**, *128*, 159–183.
(41) Nedyalkov, M.; Sultanem, C.; Benattar, J.-J. Contact angles of protein black foam films under dynamic and equilibrium conditions. *Cent. Eur. J. Chem.* **2007**, *5*, 748–765.
(42) Velev, O. D.; Campbell, B. E.; Borwankar, R. P. Effect of calcium ions and environmental conditions on the properties of β-casein stabilized films and emulsions. *Langmuir* **1998**, *14*, 4122–4130.
(43) Basheva, E. S.; Kralchevsky, P. A.; Christov, N. C.; Danov, K. D.; Stoyanov, S. D.; Blijdenstein, T. B. J.; Kim, H.-J.; Pelan, E. G.; Lips, A. Unique properties of bubbles and foam films stabilized by HFBII hydrophobin. *Langmuir* **2011**, *27*, 2382–2392.
(44) Derjaguin, B. V.; Churaev, N. V. On the question of determining the concept of disjoining pressure and its role in the equilibrium and flow of thin films. *J. Colloid Interface Sci.* **1978**, *66*, 389–398.
(45) Israelachvili, J. N. *Intermolecular and Surface Forces*; Academic Press: London, 1992.
(46) Israelachvili, J. N.; Wennerström, H. Entropic forces between amphiphilic surfaces in liquids. *J. Phys. Chem.* **1992**, *96*, 520–531.
(47) Richmond, P. Electrical forces between particles with arbitrary fixed surface charge distributions in ionic solution. *J. Chem. Soc., Faraday Trans. 2* **1974**, *70*, 1066–1073.
(48) Grimson, M. J.; Richmond, P.; Vassilieff, C. S. Electrostatic interactions in thin films. In *Thin Liquid Films*; Ivanov, I. B., Ed.; Marcel Dekker: New York, 1988; pp 275−330.
(49) Popa, I.; Gillies, G.; Papastavrou, G.; Borkovec, M. Attractive electrostatic forces between identical colloidal particles induced by adsorbed polyelectrolytes. *J. Phys. Chem. B* **2009**, *113*, 8458–8461.
(50) Meyer, E. E.; Rosenberg, K. J.; Israelachvili, J. Recent progress in understanding hydrophobic interactions. *Proc. Natl. Acad. Sci. U.S.A.* **2006**, *103*, 15739–15746.
(51) Hammer, M. U.; Anderson, T. H.; Chaimovich, A.; Shell, M. S.; Israelachvili, J. The search for the hydrophobic force law. *Faraday Discuss.* **2010**, *146*, 299–308.
(52) Gasteiger, E.; Hoogland, C.; Gattiger, A.; Duvaud, S.; Wilkins, M. R.; Appel, R. D.; Bairoch, A. Protein identification and analysis tools on the ExPASy server. In *The Proteomics Protocols Handbook*; Walker, J. M., Ed.; Humana Press: Totowa, NJ, 2005; pp 571−607.